Performance of a pervaporation system for the separation of an ethanol-water mixture using fractional condensation

Jie Liu, Jiding Li, Quan Chen and Xiaoduan Li

ABSTRACT

Polydimethylsiloxane (PDMS)/polyvinylidene fluoride (PVDF) composite membranes were fabricated and subsequently applied in ethanol recovery from an ethanol-water mixture by pervaporation (PV) using fractional condensation. The effects of feed temperature and feed flow velocity on the pervaporative properties of PDMS/PVDF composite membranes were investigated. Scanning electron microscopy (SEM) results showed that PDMS was coated uniformly on the surface of porous PVDF substrate, and the PDMS separation layer was dense with a thickness of 1.7 μm. Additionally, it was found that with increasing feed temperature, the total flux of the composite membrane increased, whereas the separation factor decreased. As the feed flow velocity increased, the total flux and separation factor increased. Besides, the permeate vapor was condensed by a two-stage fractional condenser maintained at different temperatures. The effects of the condensation conditions on fractions of ethanol-water vapor were studied to concentrate ethanol in product. The fractional condensers proved to be an effective way to enhance the separation efficiency. Under the optimum fractional condensation conditions, the second condenser showed a flux of 1,329 g/m^2 h and the separation factor was increased to 17.2. Furthermore, the long-term operation stability was verified, indicating that the PV system incorporating fractional condensation was a promising approach to separate ethanol from the ethanol-water mixture.

Key words | composite membrane, ethanol recovery, fractional condensation, pervaporation

Jie Liu (corresponding author)
Quan Chen
Xiaoduan Li
National Institute of Clean-and-Low-Carbon Energy,
Beijing 102211,
China
and
State Key Laboratory of Water Resource Protection and Utilization in Coal Mining of Shenhua Group,
Beijing 100011,
China
E-mail: *liujie_pec@nicenergy.com*

Jie Liu
Jiding Li
State Key Laboratory of Chemical Engineering,
Department of Chemical Engineering,
Tsinghua University,
Beijing 100084,
China

INTRODUCTION

Renewable bio-ethanol has been received increasing attention for the purpose of developing an alternative green energy to fossil fuels owing to its environmental and economic benefits (Kim & Dale 2004; Alvira *et al.* 2010; Sarkar *et al.* 2012). However, the concentration of bio-ethanol produced through biomass fermentation is usually less than 10 wt%, because the higher ethanol concentration will inhibit the growth of yeast cells, which will stop the fermentation process (Xia *et al.* 2012). To improve ethanol purification in the fermentation process, distillation followed by molecular sieve adsorption is usually used, which leads to both high energy consumption and capitalized cost.

Pervaporation (PV) is a promising membrane-based technology in separating thermal-sensitive compounds, azeotropes, close-boiling mixtures due to its high separation efficiency and low energy cost (Lee & Wang 1998; Li *et al.* 2016; Wang *et al.* 2016; Abdellatif *et al.* 2017; Shin *et al.* 2017). Thus, PV has become one of the most promising substitutes for conventional distillation. The mass transfer of the PV process contains three steps: selective sorption of the feed species on the membrane surface, selective diffusion through the membrane, and desorption into a vapor phase on the permeate side (Binning *et al.* 1961). Among these three steps, selective sorption and diffusion in membranes are often the rate-governing steps. To improve the total flux, the permeate side is always maintained at a pressure below the saturated pressure of a given component, either under a vacuum or by sweeping the vapor using a noncondensable carrier gas (Bruggen & Luis 2015).

Currently, almost all the commercial PV plants employ the flat-sheet and tubular membrane modules, only a few previous studies (Abou-Nemeh *et al.* 2001; Hitchens *et al.* 2001; Liu *et al.* 2015) have reported on the spiral-wound module for the PV process. Compared with the flat-sheet and tubular membrane modules, the spiral-wound configuration allows for a large membrane loading

doi: 10.2166/wst.2018.067

density (300–1,000 m^2/m^3), and can become a less expensive alternative substitute.

Many organophilic polymeric materials have been developed as ethanol perm-selective membranes, such as silicon-containing polymers, fluoro-containing polymers, and other modified polymers (Aoki 1999). Polydimethylsiloxane (PDMS) is a type of preferential hydrocarbon soluble rubber silicon, which shows ethanol-selective behavior due to its hydrophobicity and high permeability of vapors through the membrane (Yu *et al.* 2007; Zhou *et al.* 2011). Meanwhile, the low price and outstanding membrane forming property of PDMS make it easily applied in industrial PV plant. The reported separation factors of pure PDMS membranes for ethanol-water mixtures were about 7–8 (Zhou *et al.* 2011), which were insufficient for practical application. One of the popular options for producing the PV membranes is coating the polymeric layer onto the porous membrane (Zhan *et al.* 2010; Zhou *et al.* 2014a). For the selective removal of ethanol from ethanol-water mixtures by the method of PV, it is very important to select suitable support materials that have excellent membrane forming properties, high mechanical strength, and high hydrophobicity. An excellent support layer leads to much enhanced separation performance of the PV membrane. In our previous study (Zhan 2009), we studied the separation of ethanol from dilute aqueous solutions using PDMS membranes with poly-(vinylidene fluoride) (PVDF), polysulfone (PSf), polyetherimide (PEI), and polyacrylonitrile (PAN) supports. Due to PVDF's good hydrophobicity and excellent chemical stability, the PDMS/PVDF composite membrane presented the highest separation factor and outstanding structural stability in these composite membranes. Thus, a PVDF support was selected in this study. Recently, the highly effective fractional condensation has been receiving increasing attention by researchers to separate bio-oil constituents (Westerhof *et al.* 2011; Pollard *et al.* 2012; Yin *et al.* 2013; Gooty *et al.* 2014). However, the application of fractional condensation in the PV process, which can effectively improve the PV separation efficiency, has seldom been reported. A two-stage fractional condensation was used to concentrate ethanol permeate vapor due to the different boiling points of ethanol and water at the same saturated vapor pressure in this work.

In this paper, PDMS/polyvinylidene fluoride (PVDF) composite membranes were first prepared, and the PV experiments were performed with homemade available spiral-wound membrane modules. The effects of feed temperature and feed flow velocity on separation performances were studied. In the condensation process, the ethanol-water vapor flowed through a two-stage fractional condenser maintained at different temperatures to enable the collection of a higher concentration of ethanol in the final product. Finally, the stability of the PV system with fractional condensation was evaluated for 400 h of continuous operations under invariant conditions.

EXPERIMENTAL

Materials

Pure α, ω-PDMS was purchased from Beijing Chemical Reagents Corporation (Beijing, China), with an average molecular weight of 50,000 determined by GPC. N-heptane was obtained from the Jingyi Chemical Reagents Corporation (Beijing, China), and it was used as the solvent for PDMS. Dibutyltin dilaurate (DBTOL, 95%) and tetraethyl orthosilicate (TEOS, 98%) were used as the catalyst and cross-linking agent, and they were supplied by Sinopharm Chemical Reagents Corporation (Shanghai, China). The PVDF powder used for the preparation of porous membrane support in this study was Solef 1015 from Solvay Solexis Company (Brussels, Belgium). Triethyl phosphate (TEP) was used as the solvent for PVDF. TEP was reagent grade, and purchased from Beijing Chemical Reagents Corporation (Beijing, China). All chemicals were used as received unless otherwise mentioned.

Preparation of composite membranes

PVDF was dissolved in TEP to form a 15 wt% homogeneous casting solution at 65 °C, then the solution was degassed to remove bubbles for 24 h. After that, the dope solution was cast on the non-woven fabric. The flat sheet membranes were solidified by quenching in a water bath at ambient temperature for 0.5 h. Finally, the residual solvent was fully extracted with deionized water for 48 h. Flat sheet membranes were dried at room temperature.

PDMS was dissolved in n-heptane with vigorous stirring until the solution became homogeneous, then DBTOL (catalyst) and TEOS (cross-linking reagent) were added into the solution. The weight ratio of PDMS, n-hexane, DBTOL and TEOS was 100: 200: 1.2: 5. After it was degassed *in vacuo*, the resulting homogeneous PDMS solution was coated onto the PVDF membrane with a scraper. The composite membranes were first dried at room temperature for 24 h to evaporate the solvent, and were completely crosslinked in an oven at 80 °C for 5 h.

Characterization of membrane morphologies

The morphologies of the surface and cross-section of the PDMS/PVDF composite membranes were examined by scanning electron microscope (SEM, JEOL, JSM-7401F, Tokyo, Japan) using an acceleration voltage of 2 kV. The membranes were immersed in liquid nitrogen and fractured. All samples were sputtered with gold under vacuum before test.

Experimental equipment

Figure 1 shows the schematic diagram of the spiral-wound PV module. The spiral-wound module used in the PV process was much like an RO spiral-wound module. The membrane envelope, consisting of a permeate channel carrier with two flat sheets of membranes, was glued to a central core collection tube containing small holes, through which a vacuum can be applied to the inside of the membrane envelope. A feed spacer was placed on the membrane envelope, and both were wound around the core to create the module. The feed flowed through the spiral-wound module in the axial direction, and the vapor permeated radially toward the central tube under vacuum.

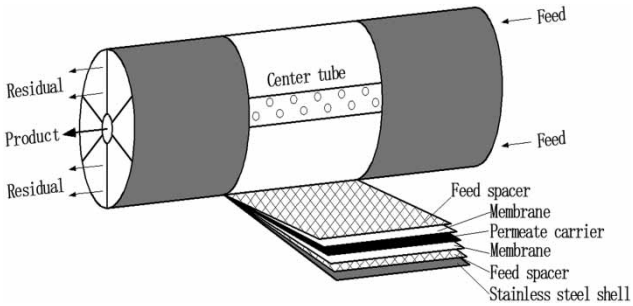

Figure 1 | Schematic diagram of spiral-wound PV module.

The spiral-wound module used in this experiment had an effective membrane surface area of 0.8 m^2, which contains 10 membrane-envelopes with a length of 225 mm glued to the central core. The width of the membrane envelope was 196 mm, and the length and diameter of the spiral-wound module were 300 mm and 63.5 mm, respectively. The thickness of the feed spacer was 0.65 mm. This short membrane envelope configuration can effectively reduce the pressure drop associated with a long permeate path length in the PV process (Liu *et al.* 2015).

The flow chart of the PV system is provided in Figure 2. The PV apparatus consisted of four parts, i.e., feed circulation, heating, condensation and vacuum. The spiral-wound membranes were positioned in a stainless-steel shell. The feed solution was continuously circulated from a feed tank to the membrane module by feed pump. The feed flow rate was controlled by adjusting the recycle flow around the feed pump, and measured by a flowmeter. A constant feed temperature was maintained by a heat exchanger, and the feed temperature was monitored by a thermometer. On the permeate side, a dry scroll vacuum pump can create limit pressures down to 50 Pa. The vacuum on the permeate side was manually controlled via a needle valve located between the membrane module and the vacuum pump inlet, and monitored by a digital vacuometer. Approximately 1.5 h was allowed for the PV system to reach steady state conditions. During the long-term operation, the concentration of ethanol in the feed tank was maintained at 9 wt%, and the spiral-wound

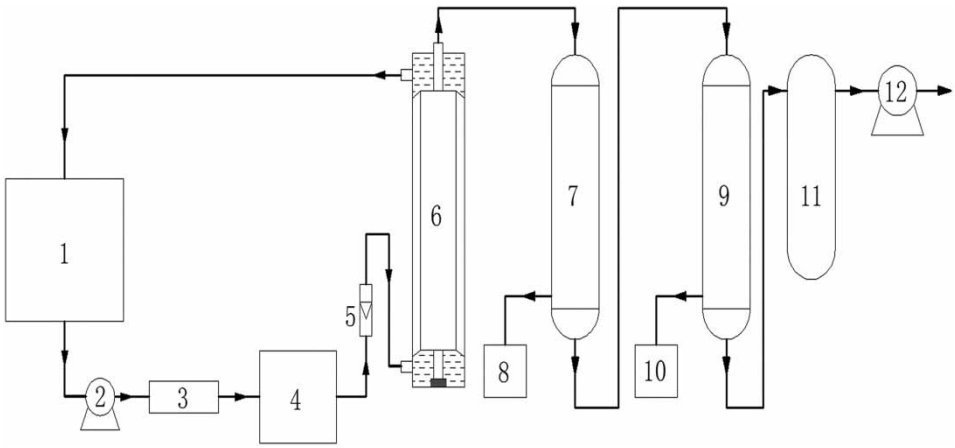

Figure 2 | Flow chart of separation of ethanol from ethanol-water mixture by PV. (1) Feed tank; (2) Feed pump; (3) Filter; (4) Heat exchanger; (5) Flowmeter; (6) Spiral-wound membrane module; (7) First condenser; (8) (10) Samplers; (9) Second condenser; (11) Balancing tank; (12) Vacuum pump.

membrane was never washed, flushed or replaced before or after the experimental run.

The condensing system was composed of a two-stage fractional condenser (condenser 7 and 9). A self-made recirculating refrigerating machine produced coolant (ethylene glycol) for the permeate condensers; the coolant temperature was maintained at −15 °C for all runs, which ensured that the majority of the vapor was collected in the condensers. The temperatures of these two condensers were controlled by adjusting the process coolant flow. The distribution of the coolant for the two-stage condensation was controlled by two needle valves at the inlet of each condenser. As shown in Figure 2, the two fractional condensers were connected in series, and the vapor stream flowed through respectively to condense the ethanol. Under the same saturated vapor pressure, the boiling point of water was much higher than that of ethanol. During the experiment, in order to separate the water present in the ethanol vapor, condenser 7 was maintained at a lower flow rate of coolant to obtain a higher temperature, so that a large amount of water was primarily condensed in condenser 7. Condenser 9 was kept at a relatively high flow rate of coolant (lower temperature) to condense the ethanol vapor, and finally the purity of the remaining ethanol was increased. The residence time of the vapors in each condenser was 1.3 s. The permeate samples were collected from two fractional condensers separately and labeled sample 1 and 2 at the end of the experiment.

Analysis

The compositions of the feed solution and permeate were analyzed by gas chromatography (Shimadzu, GC-14C, Tokyo, Japan). The PV performances were evaluated on the basis of the total flux and separation factor.

The total flux (J) was defined as the following equation:

$$J = \frac{W}{A \cdot t} \tag{1}$$

where W represented the weight of the collected permeate, A was the effective membrane area, and t was the permeation time.

The selectivity of the PV membrane was evaluated by a separation factor, which was calculated as follows (the separation factor was calculated based on total volume of permeate (1 + 2).):

$$\alpha = \frac{Y_A \cdot X_B}{X_A \cdot Y_B} \tag{2}$$

where X_A and X_B represented the ethanol and water concentrations (wt%) in the feed respectively, and Y_A and Y_B represented the ethanol and water concentrations (wt%) in the permeate.

The feed flow velocity (v_0) in the spiral-wound module was determined by:

$$v_0 = \frac{Q}{h \cdot l \cdot n} \tag{3}$$

where Q was the volume flow rate, h was the thickness of the feed spacer, l was the width of the membrane envelope, and n was the number of the membrane envelope.

As the feed flow channel was filled with spacer, the porosity of the spacer (ε) was used to adjust the feed flow velocity (the value of ε was 0.9 in this study.) (Wang *et al.* 2014):

$$v = \frac{v_0}{\varepsilon} \tag{4}$$

The Reynolds number (Re) was used to represent the flow characteristics in the spiral-wound membrane module:

$$Re = \frac{d_h \cdot v \cdot \rho}{\eta} \tag{5}$$

where d_h was the hydraulic diameter, v was the feed flow velocity, ρ was the feed density, and η was the feed viscosity. The calculation of the d_h value was reported in detail in our previous work (Wang 2014; Wang *et al.* 2014). The value of d_h in this work was 0.77 mm.

RESULTS AND DISCUSSION

Morphology of PDMS/PVDF composite membrane

Figure 3 shows the SEM photomicrographs of the PDMS/PVDF composite membrane. As shown in Figure 3(a), the surface of the composite membrane was flat and dense, and there were no pinholes or cracks. Figure 3(b)–3(d) show the whole cross-section, top part and bottom part of the cross-section of the prepared PDMS/PVDF composite membrane. The PVDF substrate had uniform bicontinuous morphology with an interconnected porous structure. It was obvious that the active PDMS layer was tightly and properly adhered on the top of the PVDF porous substrate, and the thickness of the

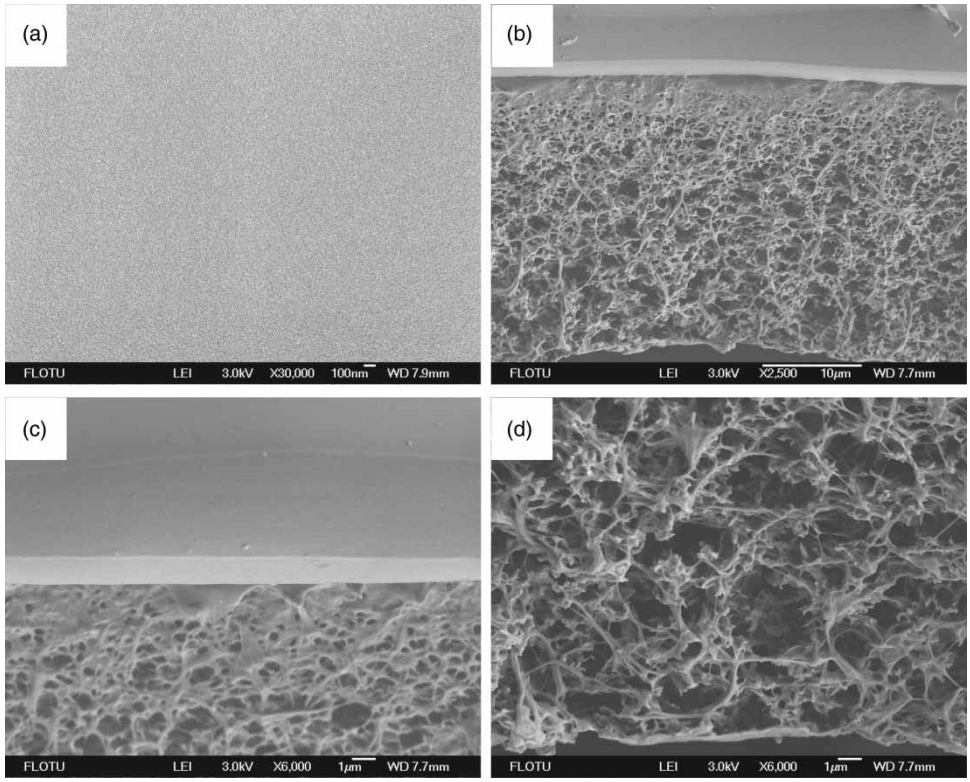

Figure 3 | SEM photomicrographs of PDMS/PVDF composite membrane. (a) Surface; (b) whole cross-section; (c) top part of cross-section; (d) bottom part of cross-section.

separation layer was almost 1.7 μm according to SEM photomicrographs. Since the top surface of the PVDF membrane was porous, the dilute PDMS homogeneous solution was liable to plugging in the pores of the PVDF membrane (Xia *et al.* 2010), leading to a transition region across the interface of the PVDF and PDMS. The formed transition region would help to improve the structural stability of the composite membrane.

Separation performance of PV system

Effect of feed temperature

The effect of feed temperature on the pervaporative properties of PDMS/PVDF composite membrane is shown in Figure 4. It was found that the feed temperature had a great influence on the transport of water and ethanol

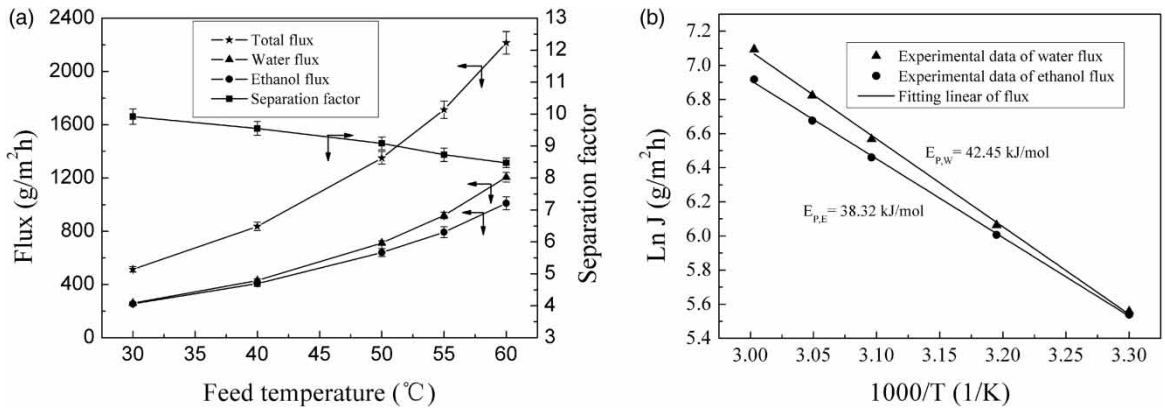

Figure 4 | Effect of feed temperature on PV properties of PDMS/PVDF composite membrane for 9.0 wt% ethanol aqueous solution with feed flow velocity 3.2 cm/s and downstream pressure 700 Pa.

molecules in the membrane. As the feed temperature was elevated from 30 to 60 °C, the total flux increased from 514 to 2,215 g/m^2 h, whereas the separation factor decreased from 9.92 to 8.48. The increase of the feed temperature resulted in an enhancement of both the water and ethanol fluxes through the membrane. This development trend was predictable. As the feed temperature increased, solubility decreased while diffusivity increased. Generally, the permeation flux increased as the feed temperature increased, but the selectivity usually decreased (Xiangli *et al.* 2007).

In the PV process, the permeate pressure was maintained much lower than the saturation pressure of a given liquid, the temperature dependence on mass transport was determined to follow Arrhenius rules (Drioli & Giorno 2009):

$$P = P_0 \exp\left(-\frac{E_P}{R \cdot T}\right) = S \cdot D \tag{6}$$

where P was the permeability coefficient, P_0 was the pre-exponential factor of permeation, E_p was the permeation activation energy for PV, T was the temperature, and R was the gas constant.

The solubility coefficient (S) and diffusion coefficient (D) were also given as the following expressions with van 't Hoff-Arrhenius rules:

$$S = S_0 \exp\left(-\frac{\Delta H_S}{R \cdot T}\right) \tag{7}$$

$$D = D_0 \exp\left(-\frac{E_D}{R \cdot T}\right) \tag{8}$$

where S_0 and D_0 were the pre-exponential factors of solubility and diffusivity, ΔH_S was the heat of sorption, and E_D was the activation energy for diffusion.

Based on Equations (6)–(8), P_0 and E_p can be provided as:

$$P_0 = S_0 \cdot D_0 \tag{9}$$

$$E_p = \Delta H_S + E_D \tag{10}$$

In the PV process, the heat of sorption (ΔH_S) was negative, and the activation energy for diffusion (E_D) was positive. When solubility was dominant for permeation as compared to diffusion, the value of permeation activation energy (E_p) must be negative and vice versa (Drioli & Giorno 2009).

The variation of the total flux (J) with temperature followed the Arrhenius equation:

$$J = J_0 \exp\left(-\frac{E_a}{R \cdot T}\right) \tag{11}$$

where J_0 was the pre-exponential factor, and E_a was the apparent activation energy of permeation. E_a can be determined from the slopes of the Ln J vs 1000/T plots, as shown in Figure 4(b).

According to Zhou *et al.*'s work (Zhou *et al.* 2014b), the permeation activation energy (E_p) can be calculated by:

$$E_p = E_a - \Delta H_V \tag{12}$$

where ΔH_V was the heat of evaporation, and the ΔH_V of ethanol and water were 41.42 kJ/mol and 42.78 kJ/mol, respectively.

As shown in Figure 4(b), the apparent activation energy (E_a) of ethanol and water were 38.32 kJ/mol and 42.75 kJ/mol, respectively. Thus, the value of E_p calculated by Equation (12) was negative. It can be concluded that the dissolution step was the rate-limiting step instead of diffusion. This result also explained why the PDMS showed ethanol-selective behavior from the ethanol-water mixture.

The change in the permeation flux may be related to two reasons (Xia *et al.* 2012). One was the increased mobility of the water and ethanol molecules and higher vapor pressure difference between two sides of the membrane, which would facilitate the diffusion process in the membrane. The other reason was that the flexibility of the polymer chains was improved with the rising temperature, which made the water and ethanol much easier to permeate the membrane. Conversely, the decrease of the separation factor was due to the higher apparent activation energy of water than that of ethanol. As shown in Figure 4(b), the apparent activation energy of ethanol was lower than that of water. A higher value of the apparent activation energy indicated an increased sensitivity to temperature (Zhou *et al.* 2014b), which meant increasing the temperature can lead to faster diffusion rate of water and more water permeate through the membrane.

Effect of feed flow velocity

The effect of feed flow velocity on the pervaporative properties of PDMS/PVDF composite membrane is shown in Figure 5. As the feed flow velocity increased, both the permeation flux and separation factor increased.

The boundary layer resistance was the main factor that influenced the mass transfer on the liquid side of the membrane surface in the PV process. As shown in Figure 6, the *Re* increased linearly with the increase in feed flow velocity.

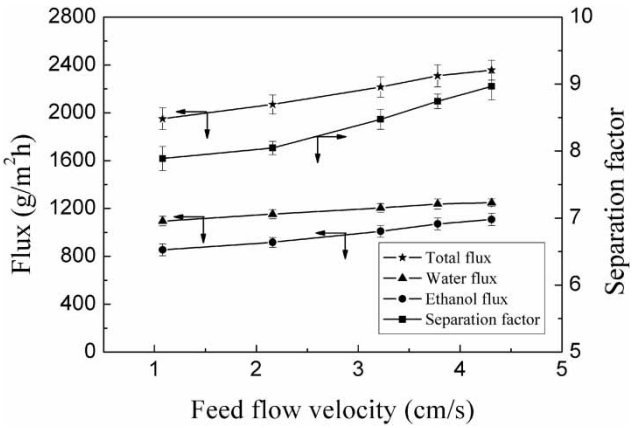

Figure 5 | Effect of feed flow velocity on PV properties of PDMS/PVDF composite membrane for 9.0 wt% ethanol aqueous solution at 60 °C with downstream pressure 700 Pa.

The higher *Re* can promote turbulence to put much shear stress on the membrane surface, which benefited the elimination of concentration polarization. Finally, the mass transfer between the bulk fluid and the membrane surface was enhanced. Because water abounded in the feed, there was hardly any resistance to water in the boundary layer. Thus, the feed flow velocity had no significant effect on the water flux but could have an obvious effect on the ethanol flux (Hickey & Gooding 1994). Moreover, as the feed flow velocity increased, more ethanol adsorbed onto the membrane surface and diffused through the membrane. As the PV experiment proceeded, the membrane was probably wetted by ethanol and the hydrophobic characteristics of the membrane surface weakened, which may have led to a higher water flux. However, the increase of water flux depended on the amount of ethanol that interacted with the membrane, and the enhanced degree of water flux was less than that of ethanol, inducing a higher separation factor (Zhou *et al.* 2014).

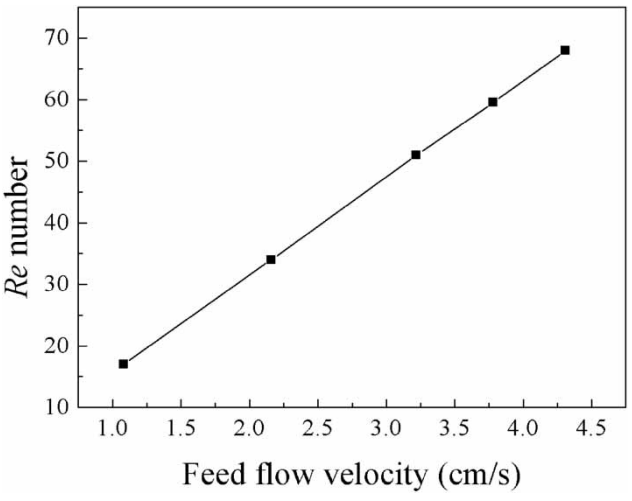

Figure 6 | Variation of *Re* with feed flow velocity in PV experiments.

Optimization of the fractional condensers

During optimizing of the condensing temperatures of the two-stage fractional condensation, all the experiments were performed at a constant operation condition (ethanol concentration of 9.0 wt%, feed temperature of 60 °C, feed flow velocity of 3.2 cm/s, and permeation side pressure of 700 Pa). Since the boiling point of water is higher than ethanol at the same saturated vapor pressure, the temperatures of the two-stage fractional condensers were varied by adjusting the coolant flow rate. In order to condense the great majority of water vapor generated in the PV process, the first condenser was operated at a relatively higher temperature with lower coolant flow rate. Throughout the experimental study, the second condenser was maintained at −10 °C for the collection of all the remaining vapor from the first condenser. Table 1 shows the water concentration, ethanol concentration, and flux collected in the first and second condenser under different condensing temperatures. As the condensing temperature of the first condenser increased from −8 °C to 2 °C, water concentration increased, ethanol concentration decreased, and flux decreased in the first condenser, whereas the reverse trend was observed in the second condenser. When the condensing temperature of the first condenser increased from 2 °C to 12 °C, the ethanol concentration in the second condenser began to decrease. An explanation for this change might be that when the condensing temperature of the first condenser ranged from −8 °C to 2 °C, most water vapor was collected in the first condenser, resulting in a higher ethanol concentration in the second condenser. Conversely, as the condensing temperature of the first condenser varied from 2 °C to 12 °C, the cooling capacity of the first condenser was not large enough to collect most water vapor, which led to the decrease of ethanol concentration in the second condenser. Considering the ethanol concentration in the final product, the condensing temperature of the first condenser at 2 °C can be selected as optimum for the collection of water-ethanol vapor. Under the optimized condensing temperature, the second condenser showed a flux of 1,329 g/m^2 h and ethanol concentration of 63.00 wt%. The separation factor of the PV system was increased to 17.2. Thus, it can be concluded that the fractional condensation was a promising cheap downstream approach to concentrate ethanol and to improve the separation efficiency of the PV process.

Table 1 | Water concentration, ethanol concentration, and flux collected in the first and second condenser under different condensing temperatures (average value of inlet and outlet temperature of coolant)

First condenser				Second condenser			
Condensing temperature (°C)	Water concentration (wt.%)	Ethanol concentration (wt.%)	Flux (g/m² h)	Condensing temperature (°C)	Water concentration (wt.%)	Ethanol concentration (wt.%)	Flux (g/m² h)
−8	52.92 ± 1.76	47.08 ± 1.76	1281 ± 47	−10	56.36 ± 1.50	43.64 ± 1.50	943 ± 36
−6	57.84 ± 1.95	42.16 ± 1.95	1173 ± 48	−10	50.49 ± 1.32	49.51 ± 1.32	1043 ± 41
−3	67.36 ± 1.71	32.64 ± 1.71	999 ± 43	−10	43.69 ± 1.75	56.31 ± 1.75	1211 ± 49
2	80.50 ± 1.54	19.50 ± 1.54	886 ± 35	−10	37.00 ± 1.29	63.00 ± 1.29	1329 ± 51
7	90.29 ± 1.39	9.71 ± 1.39	706 ± 25	−10	37.58 ± 1.57	62.42 ± 1.57	1505 ± 54
12	97.51 ± 1.01	2.49 ± 1.01	590 ± 23	−10	38.80 ± 1.43	61.20 ± 1.43	1623 ± 60

Effect of operation time

The long-term operation stability was an indispensable factor for the industrial application of PV. Figure 7 presents the detailed description of the variation of PV performance with operation time. During the 400 h of the operation stability test, only a slight fluctuation was observed in the flux and ethanol concentration in the second condenser, demonstrating that the PDMS/PVDF composite membrane had desirable structural stability and the PV system with fractional condensation possessed excellent long-term operation stability. In our study, the ethanol aqueous solution was used to simulate pretreated fermentation broth. We will further test the system with real fermentation broth and investigate the effect of fermentation by-products on PV membrane performance; future research will be more practical and comprehensive.

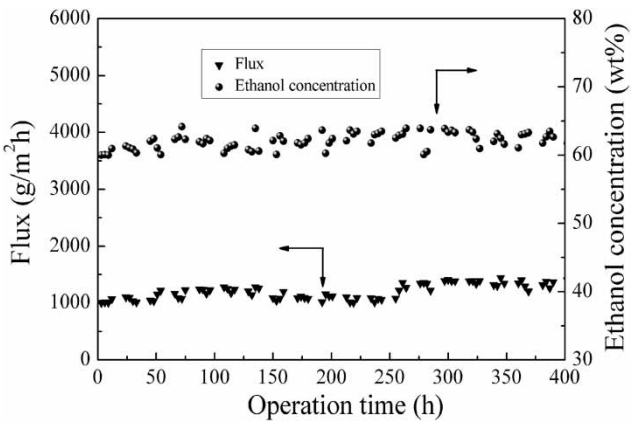

Figure 7 | Effect of operation time on PV performance of PV system with fractional condensation for 9.0 wt% ethanol aqueous solution at 60 °C with feed flow velocity 3.2 cm/s and downstream pressure 700 Pa.

CONCLUSIONS

The PDMS/PVDF composite membranes were applied in the recovery of ethanol from dilute ethanol solution by a PV system using fractional condensation. As the feed temperature increased, the total flux increased, whereas the separation factor decreased. With the increase in feed flow velocity, both the total flux and separation factor increased. The fractional condensation was an effective method to improve the separation efficiency of the PV process. Under the optimized process conditions, the second condenser exhibited a flux of 1,329 g/m² h and ethanol concentration of 63.00 wt% for 9.0 wt% ethanol aqueous solution at 60 °C with feed flow velocity 3.2 cm/s and downstream pressure 700 Pa. The separation factor of the PV system was increased to 17.2, which surpassed the limit of pure PDMS' selectivity for ethanol. Furthermore, the PV system with fractional condensation showed desirable long-term operation stability, which may be expected to be applied in the enrichment of ethanol in the fermentation industry.

ACKNOWLEDGEMENTS

The authors greatly appreciate the financial supports of the Science & Technology Innovation Funding of Shenhua Group (SHJT-15-32), National Natural Science Foundation of China (21736001, 21776153) and Science Foundation of Tsinghua University (20131089399).

REFERENCES

Abdellatif, F. H. H., Babin, J., Arnal-Herault, C., Nouvel, C., Six, J. L. & Jonquieres, A. 2017 Bio-based membranes for ethyl

tert-butyl ether (ETBE) bio-fuel purification by pervaporation. *Journal of Membrane Science* **524**, 449–459.

Abou-Nemeh, I., Majumdar, S., Saraf, A., Sirkar, K. K., Vane, L. M., Alvarez, F. R. & Hitchens, L. 2001 Demonstration of pilot-scale pervaporation systems for volatile organic compound removal from a surfactant enhanced aquifer remediation fluid II. Hollow fiber membrane modules. *Environmental Progress & Sustainable Energy* **20** (1), 64–73.

Alvira, P., Tomás-Pejó, E., Ballesteros, M. & Negro, M. J. 2010 Pretreatment technologies for an efficient bioethanol production process based on enzymatic hydrolysis: a review. *Bioresource Technology* **101** (13), 4851–4861.

Aoki, T. 1999 Macromolecular design of permselective membranes. *Progress in Polymer Science* **24** (24), 951–993.

Binning, R., Lee, R., Jennings, J. & Martin, E. 1961 Separation of liquid mixtures by permeation. *Industrial & Engineering Chemistry* **53** (1), 45–50.

Bruggen, B. V. D. & Luis, P. 2015 Chapter four–Pervaporation. *Progress in Filtration & Separation* **258** (99), 101–154.

Drioli, E. & Giorno, L. 2009 *Chapter 3. Fundamentals of Membrane Solvent Separation and Pervaporation.* Wiley-VCH Verlag GmbH & Co., Hoboken, NJ, USA.

Gooty, A. T., Li, D., Briens, C. & Berruti, F. 2014 Fractional condensation of bio-oil vapors produced from birch bark pyrolysis. *Separation & Purification Technology* **124** (6), 81–88.

Hickey, P. J. & Gooding, C. H. 1994 Mass transfer in spiral wound pervaporation modules. *Journal of Membrane Science* **92** (1), 59–74.

Hitchens, L., Vane, L. M. & Alvarez, F. R. 2001 VOC removal from water and surfactant solutions by pervaporation: a pilot study. *Separation & Purification Technology* **24** (1–2), 67–84.

Kim, S. & Dale, B. E. 2004 Global potential bioethanol production from wasted crops and crop residues. *Biomass & Bioenergy* **26** (4), 361–375.

Lee, J. F. & Wang, Y. C. 1998 Dehydration of acetic acid/water mixtures by pervaporation with a poly(4-methyl-1-pentene)/co (iii)(acetylacetonate) blend membrane. *Water Science & Technology* **38** (4–5), 463–471.

Li, Y., Shen, J., Guan, K., Liu, G., Zhou, H. & Jin, W. 2016 PEBA/ceramic hollow fiber composite membrane for high-efficiency recovery of bio-butanol via pervaporation. *Journal of Membrane Science* **510**, 338–347.

Liu, J., Chen, J., Zhan, X., Fang, M., Wang, T. & Li, J. 2015 Preparation and characterization of ZSM-5/PDMS hybrid pervaporation membranes: laboratory results and pilot-scale performance. *Separation & Purification Technology* **150**, 257–267.

Pollard, A. S., Rover, M. R. & Brown, R. C. 2012 Characterization of bio-oil recovered as stage fractions with unique chemical and physical properties. *Journal of Analytical & Applied Pyrolysis* **93** (1), 129–138.

Sarkar, N., Ghosh, S. K., Bannerjee, S. & Aikat, K. 2012 Bioethanol production from agricultural wastes: an overview. *Renewable Energy* **37** (1), 19–27.

Shin, C., Chen, X. C., Prausnitz, J. M. & Balsara, N. P. 2017 Effect of block copolymer morphology controlled by casting-solvent quality on pervaporation of butanol/water mixtures. *Journal of Membrane Science* **523**, 588–595.

Wang, T. 2014 *Mass Transport Model of Pervaporation for Removal Water From Ethanol and Flow Visualization of Fluid in Modules.* Tsinghua University, Beijing, China.

Wang, T., Zhang, Z., Ren, X., Qin, L., Zheng, D. & Li, J. 2014 Direct observation of single- and two-phase flows in spacer filled membrane modules. *Separation & Purification Technology* **125** (14), 275–283.

Wang, X., Chen, J., Fang, M., Wang, T., Yu, L. & Li, J. 2016 ZIF-7/PDMS mixed matrix membranes for pervaporation recovery of butanol from aqueous solution. *Separation & Purification Technology* **163**, 39–47.

Westerhof, R. J. M., Brilman, D. W. F., Garcia-Perez, M., Wang, Z., Oudenhoven, S. R. G., Swaaij, W. P. M. V. & Kersten, S. R. A. 2011 Fractional condensation of biomass pyrolysis vapors. *Energy & Fuels* **25** (4), 1817–1829.

Xia, Z., Li, J., Huang, J. & Chen, C. 2010 Enhanced pervaporation performance of multi-layer PDMS/PVDF composite membrane for ethanol recovery from aqueous solution. *Applied Biochemistry & Biotechnology* **160** (2), 632.

Xia, Z., Lu, J., Tan, T. & Li, J. 2012 Mixed matrix membranes with HF acid etched ZSM-5 for ethanol/water separation: preparation and pervaporation performance. *Applied Surface Science* **259** (41), 547–556.

Xiangli, F., Chen, Y., Jin, W. & Xu, N. 2007 Polydimethylsiloxane (PDMS)/ceramic composite membrane with high flux for pervaporation of ethanol-water mixtures. *Industrial & Engineering Chemistry Research* **46** (7), 2224–2230.

Yin, R., Liu, R., Mei, Y., Fei, W. & Sun, X. 2013 Characterization of bio-oil and bio-char obtained from sweet sorghum bagasse fast pyrolysis with fractional condensers. *Fuel* **112** (10), 96–104.

Yu, N., Ando, T. & Yun, C. M. 2007 Syntheses of siloxane-grafted aromatic polymers and the application to pervaporation membrane. *Reactive & Functional Polymers* **67** (11), 1252–1263.

Zhan, X. 2009 *Preparation and Pervaporation Performance of Ethanol Permselective Silicone Membranes.* Tsinghua University, Beijing, China.

Zhan, X., Li, J., Huang, J. & Chen, C. 2010 Enhanced pervaporation performance of multi-layer PDMS/PVDF composite membrane for ethanol recovery from aqueous solution. *Applied Biochemistry & Biotechnology* **160** (2), 632.

Zhou, H., Su, Y., Chen, X. & Wan, Y. 2011 Separation of acetone, butanol and ethanol (ABE) from dilute aqueous solutions by silicalite-1/PDMS hybrid pervaporation membranes. *Separation & Purification Technology* **79** (3), 375–384.

Zhou, H., Lv, L., Liu, G., Jin, W. & Xing, W. 2014a PDMS/PVDF composite pervaporation membrane for the separation of dimethyl carbonate from a methanol solution. *Journal of Membrane Science* **471**, 47–55.

Zhou, H., Shi, R. & Jin, W. 2014b Novel organic–inorganic pervaporation membrane with a superhydrophobic surface for the separation of ethanol from an aqueous solution. *Separation & Purification Technology* **127** (1), 61–69.

First received 17 August 2017; accepted in revised form 3 February 2018. Available online 15 February 2018